

# Isospin purity of T=1 states in the A=38 nuclei studied via lifetime measurements in $^{38}\text{K}$

F. M. Prados Estévez,<sup>1</sup> A. M. Bruce,<sup>1</sup> M. J. Taylor,<sup>1,\*</sup> H. Amro,<sup>2,†</sup> C. W. Beausang,<sup>2,‡</sup> R. F. Casten,<sup>2</sup> J. J. Ressler,<sup>2</sup> C. J. Barton,<sup>3,\*</sup> C. Chandler,<sup>4</sup> and G. Hammond<sup>4,\*</sup>

<sup>1</sup>*School of Engineering, University of Brighton, Brighton BN2 4GJ, UK.*

<sup>2</sup>*Wright Nuclear Structure Laboratory,*

*Yale University, New Haven, CT 06520, USA.*

<sup>3</sup>*CLRC Daresbury Laboratory, Daresbury, Warrington WA4 4AD, UK.*

<sup>4</sup>*School of Chemistry and Physics, Keele University, Staffordshire, ST5 5BG, UK.*

(Dated: January 18, 2007)

## Abstract

The Doppler Shift Attenuation Method has been used to measure lifetimes for levels in  $^{38}\text{K}$  at excitation energies of 1698, 2404, 2830, 2996 and 3671 keV, populated using the  $^{40}\text{Ca}(\text{d},\alpha)^{38}\text{K}$  reaction at a beam energy of 4.5 MeV. Values of 109(29), 95(22), 457(63), 130(40) and 160(50) fs respectively were measured and are compared with previous values obtained using different stopping powers. The matrix element for the transition between the  $J^\pi = 2_{T=1}^+$  and  $0_{T=1}^+$  states in this  $T_z=0$  nucleus is compared with the analogous transition in the other nuclei in the T=1 triplet,  $^{38}\text{Ca}$  ( $T_z=-1$ ) and  $^{38}\text{Ar}$  ( $T_z=+1$ ), and with the results of shell-model calculations.

PACS numbers: 21.10.-k, 21.10.Tg, 21.60.Cs, 23.20.Js, 27.30.+t

---

\*Current address: Department of Physics, University of York, Heslington, York, YO10 5DD, UK.

†Current address: Department of Physics, University of Notre Dame, Notre Dame, IN 46556, USA.

‡Current address: Department of Physics, University of Richmond, Richmond, VA 23173, USA.

## I. INTRODUCTION.

Evidence that the nucleon-nucleon force is charge independent can be found in the energy spectra of nuclei in a  $T=1$  isobaric triplet where states with the same spin, parity and quite similar energy are observed. An example is shown in Figure 1 where the first excited  $2_{T=1}^+$  states for members of the  $A=38$  isobaric triplet ( $^{38}_{18}\text{Ar}_{20}(T_z=+1)$ ,  $^{38}_{19}\text{K}_{19}(T_z=0)$  and  $^{38}_{20}\text{Ca}_{18}(T_z=-1)$ ) are plotted.  $T_z$  is defined as  $(N-Z)/2$ .

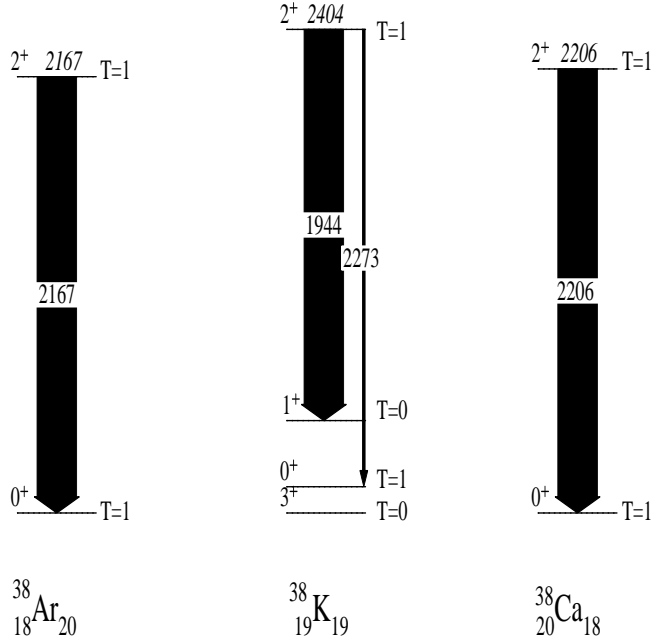


FIG. 1: The first excited  $2_{T=1}^+$  states for nuclei in the  $A=38$  isobaric triplet.

A more rigorous test of the wavefunctions of the  $2_{T=1}^+$  states can be made by considering the transition probability of transitions to the  $0_{T=1}^+$  states. The reduced transition probability is related to the partial  $\gamma$ -ray lifetime ( $\tau_\gamma$ ) by:

$$B(E2, E_i \rightarrow E_f) = \frac{1}{1.22 \times 10^9 E_\gamma^5 \times \tau_\gamma} (e^2 (fm)^4) \quad (1)$$

where  $\tau_\gamma$  is in seconds and  $E_\gamma$  is the transition energy, measured in MeV, and to the matrix element ( $M_p$ ) by:

$$M_p = [(2J_i + 1) \times B(E2, E_i \rightarrow E_f)]^{1/2} (e(fm)^2). \quad (2)$$

Figure 2 shows the values of  $M_p$  for the  $2_{T=1}^+ \rightarrow 0_{T=1}^+$  transitions for members of the  $A=22$ -42  $T=1$  triplets plotted as a function of isospin  $T_z$ . Two features are immediately evident

from these plots, one is that for all triplets, with the exception of  $A = 38$ , the values of  $M_p$  decrease as  $T_z$  increases. The second is that the data point for  $^{38}\text{K}$  is two standard deviations from the value expected by assuming a linear dependence. This latter point was highlighted in a recent paper by Cottle *et al* [4].

The data presented in Figure 2 hints at broken isospin symmetry in the  $A=38$  triplet and has provided the motivation to re-measure the value of the matrix element in  $^{38}\text{K}$ . The value plotted in Figure 2 for  $^{38}\text{K}$  is taken from the weighted average of three measurements of the lifetime of the  $2_{T=1}^+$  state ( $72 \pm 17$  fs) [7–9] and the branching ratios for the 2273 keV ( $6 \pm 2$ ) and 1944 keV ( $94 \pm 2$ ) [7, 10] transitions from this state as shown in Figure 1. The Doppler Shift Attenuation Method (DSAM) was used to make previous measurements of the lifetime of excited states in  $^{38}\text{K}$  [7–9] and was considered the most appropriate tool for this study. The existence of an yrast, isomeric ( $\tau = 32(1)\mu\text{s}$ )  $J^\pi = 7^+$  state at  $\sim 3.5$  MeV [11] precludes the use of a fusion-evaporation reaction to populate the state of interest. Therefore the  $(d,\alpha)$  reaction was used.

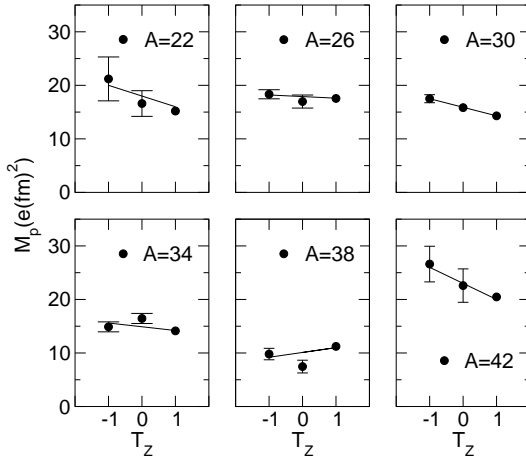


FIG. 2: Matrix elements for the  $2_{T=1}^+ \rightarrow 0_{T=1}^+$  transition in  $T=1$  triplets from  $A=22$  to  $A=42$ . The straight lines correspond to the best fits calculated using the least-squares method. Data taken from [1–6]. For some nuclei ( $T_z=1$  and  $^{30}\text{P}$ ) the error bar is smaller than the data point.

## II. EXPERIMENTAL PROCEDURE.

States in  $^{38}\text{K}$  were populated using the  $^{40}\text{Ca}(d,\alpha)$  reaction at a beam energy of 4.5 MeV. Given that the reaction has a positive  $Q$  value, the beam energy was chosen to be as low

as possible, in order to minimise side feeding. The beam of deuterons was accelerated by the ESTU tandem accelerator [12] at the Wright Nuclear Structure Laboratory at Yale University. The  $220 \mu\text{g}/\text{cm}^2$   $^{40}\text{Ca}$  target was supported on a  $1 \text{ mg}/\text{cm}^2$  Ni backing and had a flash of gold on the front face to prevent oxidation. The deuteron beam lost  $\sim 15 \text{ keV}$  in reaching the centre of the target [13] and the maximum  $^{38}\text{K}$  recoil energy was calculated using the reaction kinematics code CatKin [14] to be 2 MeV. A recoil of this energy would be stopped in the nickel backing.

$\gamma$  rays were measured in an array of 8 Clover detectors, 4 at an angle in the horizontal plane ( $\theta$ ) with respect to the beam direction of  $140^\circ$  with angles in the vertical plane ( $\phi$ ) of  $0^\circ$ ,  $90^\circ$ ,  $180^\circ$  and  $270^\circ$  and 4 with  $\theta = 90^\circ$  and  $\phi = 80^\circ$ ,  $160^\circ$ ,  $200^\circ$  and  $280^\circ$ . Energy and efficiency calibrations were performed with sources of  $^{152}\text{Eu}$  and  $^{226}\text{Ra}$ . The  $^{226}\text{Ra}$  source was used because it emits  $\gamma$  rays up to 2446 keV.

The SCARY array of Solar cells [15] was used to detect the  $\alpha$  particles. It consists of 8 detectors centred at  $\theta = 154^\circ$  with  $\phi$  angles of  $0^\circ, 45^\circ, 90^\circ, 135^\circ, 180^\circ, 225^\circ, 270^\circ$  and  $315^\circ$ . The solar cells were calibrated with a  $^{228}\text{Th}$  source and were measured to have FWHM values of 150 keV at 5.4 MeV before the experiment, degrading slightly to 200 keV after the experiment.

Two types of data were collected simultaneously:

- Particle- $\gamma$  coincidence events where a  $\gamma$  ray and a particle were observed within 400 ns of each other.
- $\gamma$ - $\gamma$  coincidence events in which the energy of each of a pair of  $\gamma$  rays observed within 100 ns was recorded.

Events were written to disk for subsequent off-line analysis where they were sorted using the CSCAN analysis package [16] into a variety of matrices. The Radware analysis software package [17] has been used to analyse the data. Data from the particle- $\gamma$  coincidence events was used to construct 9 particle-energy,  $\gamma$ -ray energy matrices, one for each of the composite angles between the solar cells and germanium detectors. The angles are  $75^\circ$ ,  $83^\circ$ ,  $95^\circ$ ,  $103^\circ$ ,  $123^\circ$ ,  $127^\circ$ ,  $137^\circ$ ,  $148^\circ$  and  $155^\circ$ . Data from the  $\gamma$ - $\gamma$  coincidence events was used to construct a  $\gamma$ - $\gamma$  matrix.

The lifetimes of the states were deduced by observing the  $\gamma$ -ray Doppler shift which is related to the slowing down time of the recoil in the target backing. The Doppler effect is

given by

$$E_\gamma = E_o \frac{\sqrt{1 - \frac{v^2}{c^2}}}{1 - \frac{v}{c} \cos \theta} \approx E_o \left(1 + \frac{\bar{v}}{c} \cos \theta\right) \quad (3)$$

where  $\theta$  is the angle between the direction of the recoil and the direction of the  $\gamma$ -ray emission,  $E_o$  is the  $\gamma$ -ray energy when it is emitted when the nucleus is at rest and  $E_\gamma$  is the energy of the  $\gamma$  ray emitted when the nucleus is moving. In the DSAM, the average velocity  $\bar{v}$  of the recoiling nucleus when the level decays is determined by plotting the  $\gamma$ -ray energy  $E_\gamma$  as a function of  $\cos \theta$ . The unshifted energy ( $E_o$ ) and the average velocity  $\bar{v}$  can then be obtained from the slope and intercept of this graph as shown in Equation 3.  $\bar{v}$  is related to the lifetime of decay of the excited state via the Doppler-Shift Attenuation Factor  $F(\tau)$  [18] which is given by

$$F(\tau) = \frac{\bar{v}}{v_o} = \frac{1}{v_o \tau} \int_0^\infty v(t) \exp(-t/\tau) dt \quad (4)$$

where  $v_o$  is the initial recoil velocity,  $v(t)$  is the recoil velocity as a function of time during the slowing down process in the backing material and  $\tau$  is the lifetime of the state. The initial velocity ( $v_o$ ) for each level was determined using CatKin [14]. In this work the velocity profiles have been obtained using a version of Dechist [19] modified to include the SRIM [13] stopping powers and the integration done numerically. The validity of the method was checked by considering the lifetimes of states in  $^{56}\text{Co}$  produced via the  $(d,\alpha)$  reaction on the  $^{58}\text{Ni}$  target backing. Values of lifetimes obtained for the 1931, 2062, 2307, 2360 and 2637 keV levels in  $^{56}\text{Co}$  were in agreement with previous work [20]. Further details can be found in [21].

### III. EXPERIMENTAL RESULTS.

The partial level scheme of  $^{38}\text{K}$  observed in this experiment is shown in Figure 3. Table I lists the  $\gamma$ -ray energies measured in the projection of a particle- $\gamma$  matrix.  $\gamma$ -ray branching ratios have been measured by fitting the angular distribution data and allowing the population of the substates in the reaction and the  $\gamma$ -ray intensity to vary as outlined in [22]. The intensities quoted are in broad agreement with those in Collins *et al.* [7] and Hasper *et al.* [10] except for the transitions depopulating the 3693 keV level where Collins *et al.* have the 1044 keV transition being half as intense as the 1076 keV transition. This is opposite to

what is observed in the current work. For the 2404 keV level, Collins *et al.* [7] and Hasper *et al.* [10] quote branching ratios of 100/6.4 and 100/7.5 for the 1944 and 2273 keV transitions respectively. Neither of the papers observed evidence for the 705 and 2404 keV transitions and, in the current work, a detailed analysis of the  $\gamma$ - $\gamma$  coincidence matrix was performed to get upper limits for these transitions.

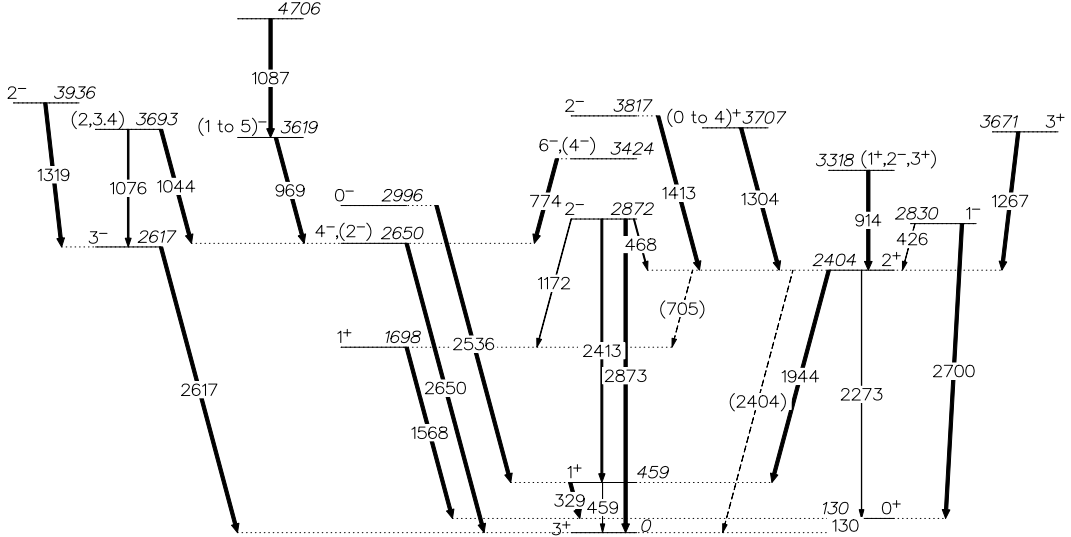


FIG. 3: Partial level scheme for  $^{38}\text{K}$  showing the excited states and transitions observed in this work.

The particle- $\gamma$  coincidence data was used to set gates on the  $\alpha$ -particle energy so that the contribution from side-feeding could be eliminated. Figure 4 shows the particle spectra measured in coincidence with the 2700, 1568 and 329 keV transitions. The spectra give an indication of the quality of the data and the  $\alpha$ -particle energies measured are consistent with those calculated using CatKin [14]. Figure 4c) is double peaked since the 459 keV level (from which the 329 keV transition decays) is fed both directly and indirectly from higher lying states. Setting a gate on  $\alpha$ -particle energies higher than  $\sim 5.5$  MeV eliminates the contribution to the measured lifetime of the level from side-feeding. Analysis of the particle- $\gamma$  data indicated that the statistics were sufficient to extract centroid shifts for seven transitions, namely the 426, 1267, 1568, 1944, 2273, 2536 and 2700 keV transitions depopulating the five states listed in column 1 of Table II. Figure 5 shows the measured energy of the 1944 keV transition as a function of  $\cos\theta$ . The  $F(\tau)$  attenuation factors extracted using Equations 3 and 4 are listed in Table II. The attenuation factors for the 2404 and 2830 keV excited states were determined by the weighted average between the

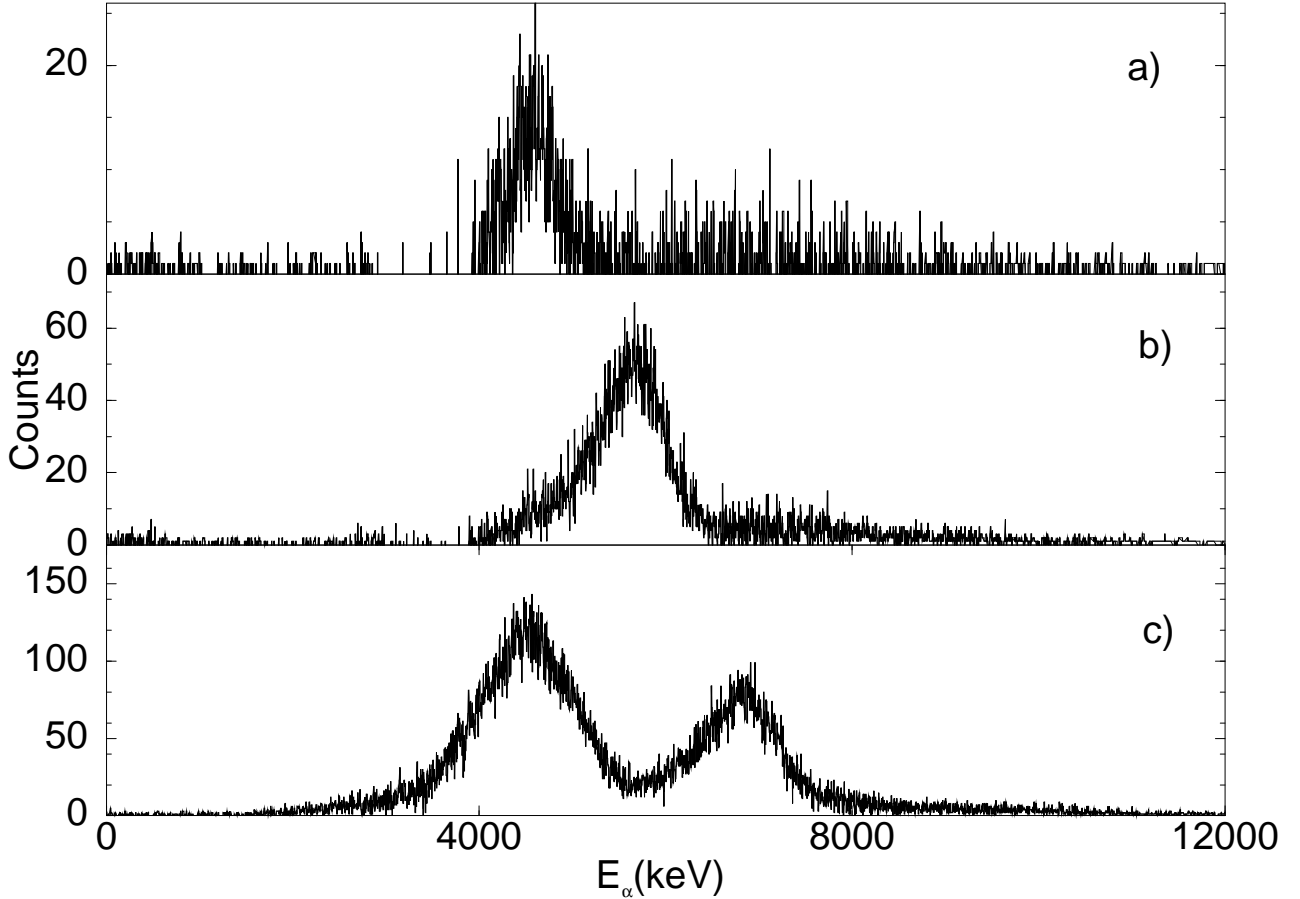


FIG. 4: Particle spectra obtained by gating on a) the 2700 keV b) the 1568 keV and c) the 329 keV transitions depopulating the 2830, 1698 and 459 keV levels respectively.

attenuation factors measured for the 1944 and 2273 keV transitions from the 2404 keV state and the 426 and 2700 keV transitions from the 2830 keV state.

Table III lists the lifetimes extracted using Equation 4 along with previous results from Collins *et al.* [7], Hasper *et al.* [8] and Engmann *et al.* [9]. Collins *et al.* [7] used the  $(d,\alpha)$  reaction but with a beam energy of 7.84 MeV and a target consisting of  $100 \mu\text{g}/\text{cm}^2$  natural calcium on a  $1 \text{ mg}/\text{cm}^2$  silver backing. Hasper *et al.* [8] also used the  $(d,\alpha)$  reaction but with a deuteron energy (4.421 MeV) and a target composition ( $320 \mu\text{g}/\text{cm}^2$  natural calcium on a  $1 \text{ mg}/\text{cm}^2$  nickel backing) very similar to the current work. Engmann *et al.* [9] used the  $^{39}\text{K}(^{3}\text{He},\alpha)^{38}\text{K}$  reaction with a beam energy of 9.0 MeV and a target consisting of  $700 \mu\text{g}/\text{cm}^2$  natural KBr evaporated onto a  $500 \mu\text{g}/\text{cm}^2$  gold foil. Hence it is only the  $F(\tau)$  values of Hasper and Smith [8] with which a meaningful comparison can be made and, in general, the values measured in the current work are in agreement with those of Hasper and Smith.

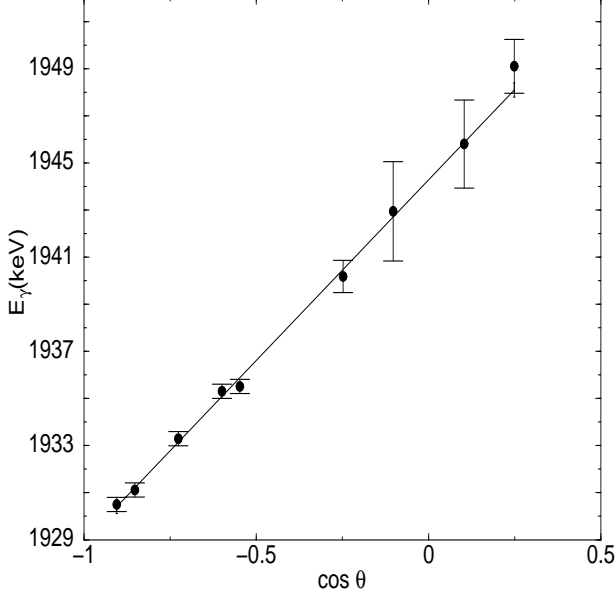


FIG. 5: The measured energy of the 1944 keV transition from the 2404 keV state as a function of  $\cos\theta$ . The straight line corresponds to the best fit.

Despite this, the lifetimes extracted in the current work are on average  $\sim 25\%$  larger than those of Hasper and Smith [8] who used nuclear and electronic stopping-power theories of Lindhard *et al.* [24] and Blaugrund's approximation of the scattering angle [25]. Analysis of these stopping powers [21] has shown that they are  $\sim 50\%$  larger than the values calculated by SRIM [13] in the energy region of interest, thus giving a shorter lifetime for essentially the same  $F(\tau)$  value. The final column of Table III lists the weighted average values of the lifetimes. Using the value of  $80 \pm 13$  fs for the lifetime of the 2404 keV state and the branching ratios listed in Table I, a matrix element of  $8.7 \pm 0.9$  for the  $2_{T=1}^+ \rightarrow 0_{T=1}^+$  transition is obtained.

#### IV. DISCUSSION.

Shell model calculations for  $^{38}\text{K}$  were done using the Antoine shell model code [26] with the CWH [27], USD [28] and IOKIN.SDPF.SI35 [29] interactions. Figure 6 shows the comparison between the empirical positive-parity levels below 2.5 MeV and the results of these calculations. The CWH and USD interactions only include the  $N(Z)=8$  to 20 shell and therefore calculations for  $^{38}\text{K}$  ( $N=Z=19$ ) have a restricted space when these interactions are used. The IOKIN.SDPF.SI35 interaction has been developed to describe nuclei with  $N>20$

such as  $^{38}\text{Cl}$  and  $^{40,41}\text{K}$  [29] and, in addition to levels in the  $N(Z)=8$  to 20 shell, includes the  $f_{7/2}$ ,  $p_{3/2}$ ,  $f_{5/2}$  and  $p_{1/2}$  orbits. In the current work this valence space was truncated to allow excitation from the sd shell only into the  $f_{7/2}$  orbit. The rightmost 3 columns in the figure show the result of allowing 0,2 and 4 particles respectively across the  $A = 40$  shell gap. Identical results could be obtained by allowing 1,3 or 5 particles across the shell gap indicating that the particles prefer to move in pairs. The reduced  $\chi^2$  (defined as  $\sum_{i=1}^N (E_i^{\text{exp}} - E_i^{\text{th}})^2 / (1000 \cdot N)$ ) between the experimental levels and the theoretical calculations is given at the top of the figure for each interaction. The best agreement with the experimental values is achieved by the configuration which allowed a maximum of 2 excitations from the sd shell to the  $1f_{7/2}$  orbit. It might be expected that better results would be obtained as the number of allowed excitations increases. The fact that this is not observed could be because the IOKIN.SDPF.SI35 interaction was optimised to describe the neutron-rich nuclei around  $N=28$  [29].

$\chi^2 =$	11.5	14.0	32.0	3.8	10.4	
$2^+$ <u>2403.7</u>	$2^+$ <u>2510.3</u>	$2^+$ <u>2323.7</u>	$2^+$ <u>2438.6</u>	$2^+$ <u>2323.9</u>	$2^+$ <u>2280.9</u>	
$1^+$ <u>1698.3</u>	$1^+$ <u>1853.9</u>	$1^+$ <u>1720.8</u>	$1^+$ <u>1712.4</u>	$1^+$ <u>1585.7</u>	$1^+$ <u>1557.5</u>	
$1^+$ <u>459.4</u>	$0^+$ <u>484.5</u>	$1^+$ <u>634.7</u>	$1^+$ <u>685.3</u>	$0^+$ <u>458.4</u>	$1^+$ <u>457.5</u>	
$0^+$ <u>130.3</u>	$1^+$ <u>276.1</u>	$0^+$ <u>310.5</u>		$0^+$ <u>118.2</u>	$1^+$ <u>398.8</u>	
$3^+$ <u>0.0</u>	$3^+$ <u>15.3</u>					
occupation= 0			occupation= 2		occupation= 4	
Experiment	CWH	USD	IOKIN.SDPF.SI35			

FIG. 6: Positive-parity levels below 2.5 MeV in  $^{38}\text{K}$  compared with the results of shell-model calculations (see text for details).

Figure 7 shows the matrix elements for the  $A=38$  triplet compared with the results of shell-model calculations using the USD interaction (left) and the IOKIN.SDPF.SI35 inter-

action allowing 2 particles across the A=40 shell gap (right). The calculations used  $e_n = 0.5$  and  $e_p = 1.5$  but have been normalised in each case to the empirical value for  $^{38}\text{Ar}$ . Although Figure 6 indicated that the best agreement for the level energies could be obtained with the IOKIN.SDPF.SI35 interaction and allowing 2 particles across the A=40 shell gap, Figure 7 shows that there is little difference in the predictions in terms of matrix elements and indeed the calculated  $M_p$  values are almost identical for all five situations shown in Figure 6. This indicates that the structure of the T=1 states is not affected strongly by the different interactions. None of the calculations is able to explain the value of the matrix element for  $^{38}\text{Ca}$  which is  $\sim 150\%$  larger than predicted.

The value for  $^{38}\text{Ar}$  is obtained from a measurement by Speidel *et al.* [3] using the Doppler Shift Attenuation Method following the  $^{12}\text{C}(^{34}\text{S}, ^8\text{Be})^{38}\text{Ar}$  reaction at a beam energy of 67 MeV. The value of  $B(E2:0_{g.s.}^+ \rightarrow 2_1^+)$  which they measure ( $122 \pm 3 \text{ e}^2\text{fm}^4$ ) is compared with a value of  $171 \text{ e}^2\text{fm}^4$ , calculated [3] using full sd shell model calculations with the WBT interaction [30] and effective charges of  $e_n = 0.5$  and  $e_p = 1.5$ . Indeed, both the value for  $^{38}\text{Ar}$  and the one for  $^{38}\text{K}$  are in agreement with the results of calulations [31] using the Chung and Wildenthal interaction [32].

The value for  $^{38}\text{Ca}$  is obtained from a measurement of  $B(E2:0_{g.s.}^+ \rightarrow 2_1^+) = 96 \pm 21 \text{ e}^2\text{fm}^4$  via intermediate energy Coulomb excitation of a beam of radioactive  $^{38}\text{Ca}$  [4]. This value equates to  $B(E2:2_1^+ \rightarrow 0_{g.s.}^+) = 19.2 \pm 4.2 \text{ e}^2\text{fm}^4$  and an  $M_p$  value of  $10 \pm 1 \text{ efm}^2$ . It is, however, of note that, in ref. [4], the authors comment that the B(E2) value to the second excited  $2^+$  state is of the same order of magnitude to that observed to the first. This is unexpected due to the different nature of the two  $2^+$  states (the second of which is a member of a deformed band built on the 3.057 MeV  $0^+$  state) but is interpreted as implying modest mixing between the 3.057 MeV  $0^+$  state and the ground state. It could be that instead the mixing is between the two  $2^+$  states thus affecting the value of the matrix element measured for the  $2_{T=1}^+ \rightarrow 0_{T=1}^+$  transition. However this seems an unlikely solution given that the energy of the  $2^+$  state shown in Figure 1 is not much shifted from where the systematics suggest it should be and indeed, it would not explain why the observed B(E2) value is larger than that expected from systematics or from the results of shell-model calculations.

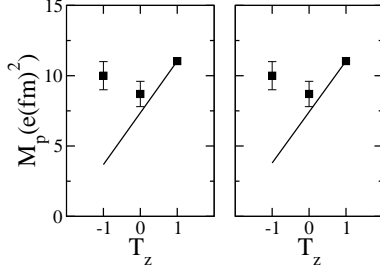


FIG. 7: Comparison between the empirical matrix elements for the  $2_{T=1}^+ \rightarrow 0_{T=1}^+$  transition for the  $A=38$  isobaric triplet and the results of shell model calculations using left: the USD interaction and right: the IOKIN.SDPF.SI35 interaction and allowing 2 particles across the  $A=40$  shell gap. The error bar for the  $T_z=1$  data point ( $^{38}\text{Ar}$ ) is smaller than the symbol.

## V. CONCLUSIONS

The lifetimes of 5 excited states in  $^{38}\text{K}$  have been measured using the DSAM technique following the  $(\text{d},\alpha)$  reaction. The values measured are in general agreement with previous work [7–9]. This is particularly important for the 2404 keV  $J^\pi = 2^+$  state since a recent measurement [4] in  $^{38}\text{Ca}$  suggested that the previous value for the matrix element for the  $2_{T=1}^+ \rightarrow 0_{T=1}^+$  transition in  $^{38}\text{K}$  did not fit with the systematics of the  $T=1$ ,  $A=38$  nuclei. This re-measurement confirms the value for  $^{38}\text{K}$  which is in agreement with both the systematics and the results of shell-model calculations using a range of interactions and model spaces. This measurement therefore adds to the intrigue of understanding the structure of the  $J^\pi = 2_{T=1}^+$  states in the  $A=38$  nuclei.

### Acknowledgements

The visitors to the WNSL would like to thank the technical and academic staff for their assistance and hospitality. This work is supported by the UK EPSRC and F.M.P.E. and G.H. acknowledge receipt of EPSRC postgraduate studentships. Yale University is supported by the US DOE under grant no. DE-FG02-91ER-40609. Dr. Lipski at the University of Stony

Brook is thanked for preparing the targets.

---

- [1] P.M.Endt, Nucl. Phys. **A633** 1, (1998).
- [2] P.D.Cottle *et al.*, Phys. Rev. **C64** 057304, (2001).
- [3] K.-H.Speidel *et al.*, Phys. Lett. **B632** 207, (2006).
- [4] P.D.Cottle *et al.*, Phys. Rev. **C60** 031301(R), (1999).
- [5] B.Singh and J.A.Cameron, Nucl. Data Sheets **92** 1, (2001).
- [6] J.N.Orce *et al.*, Phys. Rev. **C70** 014314, (2004).
- [7] W.K.Collins *et al.*, Phys. Rev. **C11** 1925, (1975).
- [8] H.Hasper and P.B.Smith, Phys. Rev. **C8** 2240, (1973).
- [9] R.Engmann *et al.*, Nucl. Phys. **A162** 295, (1971).
- [10] H.Hasper *et al.*, Phys. Rev. **C5** 1261, (1972).
- [11] A.Iordăchescu *et al.*, Phys. Lett. **B48** 28, (1974).
- [12] H.R.McK.Hyder *et al.*, Nucl. Ins. Meth. **A268** 285, (1988).
- [13] J.F.Ziegler and J.P.Biersack. SRIM © SRIM.com, 2003.
- [14] W.N.Catford Catkin V2.00©The relativistic kinematics program. Technical report, 2000
- [15] C.W.Beausang *et al.*, Nucl. Ins. Meth. **A452** 431, (2000).
- [16] J.J.Ressler *et al.*, CSCAN manual, Yale University, 2003.
- [17] D.C.Radford, Nucl. Ins. Meth. **A361** 297, (1995).
- [18] S.Devons, *The measurement of very short lifetimes in nuclear spectroscopy*. Springer-Verlag, 1960.
- [19] J.C.Wells *et al.*, *Lineshape: a computer program for Doppler-broadened lifetime analysis* Oak Ridge internal report number 6689, 1996.
- [20] W.D.Kampp and S.Buhl, Z.Physik **A284** 117, (1978).
- [21] F.M.Prados Estevez, PhD Thesis, University of Brighton, 2006.
- [22] R.D.Gill, *Gamma-ray angular correlations*. Academic Press Inc. London, New York and San Francisco, 1975.
- [23] R.B.Firestone and V.S.Shirley, *Table of Isotopes* John Wiley and Sons, 1996.
- [24] J.Lindhard *et al.*, Kgl. Dan. Vidensk. Selsk. Mat.-Fys. Medd. **33** No. 4, (1963).
- [25] A.E.Blaugrund, Nucl. Phys. **88** 501, (1966).

- [26] E.Caurier and F.Nowacki, Acta Physica Polonica **B30** 705, (1999).
- [27] B.H.Wildenthal in *Elementary Modes of excitation in Nuclei*. Proceedings of the International School of Physics Enrico Fermi, North-Holland, Amsterdam, 1977.
- [28] B.H.Wildenthal Prog. Part. Nucl. Phys. **11** 5, (1984).
- [29] J.Retamosa, E.Caurier, F.Nowacki and A.Poves, Phys. Rev. **C55** 1266, (1996).
- [30] E.K.Warburton and B.A.Brown, Phys. Rev. **C46** 923, (1992).
- [31] B.A.Brown *et al.*, Phys. Rev. **C26** 2247, (1982).
- [32] B.A.Brown, W.Chung and B.H.Wildenthal, Phys. Rev. **C21** 2600, (1980).

$J_i^\pi$	$J_f^\pi$	$E_i$ (keV)	$E_f$ (keV)	$E_\gamma$ (keV)	$I_\gamma$
1 <sup>+</sup>	0 <sup>+</sup>	459.4(4)	130.3(5)	329.1(2)	100.0(3)
	3 <sup>+</sup>		0	459.4(4)	1.5(3)
1 <sup>+</sup>	0 <sup>+</sup>	1698.3(6)	130.3(5)	1568.0(4)	
2 <sup>+</sup>	1 <sup>+</sup>	2403.7(6)	1698.3(6)	705.4(8)	<6
	1 <sup>+</sup>		459.4(4)	1944.3(5)	100(3)
	0 <sup>+</sup>		130.3(5)	2273.1(14)	10(3)
	3 <sup>+</sup>		0	2403.7(3)	<5
3 <sup>-</sup>	3 <sup>+</sup>	2616.6(4)	0	2616.6(4)	
4 <sup>-</sup> ,(2 <sup>-</sup> )	3 <sup>+</sup>	2649.6(4)	0	2649.6(4)	
1 <sup>-</sup>	2 <sup>+</sup>	2830.2(6)	2403.7(6)	426.3(4)	10.5(5)
	0 <sup>+</sup>		130.3(5)	2700.3(8)	100.0(5)
2 <sup>-</sup>	2 <sup>+</sup>	2872.3(3)	2403.7(6)	468.2(3)	31.4(5)
	1 <sup>+</sup>		1698.3(6)	1172.1(8)	17(1)
	1 <sup>+</sup>		459.4(4)	2413.1(5)	57.8(7)
	3 <sup>+</sup>		0	2872.7(4)	100(1)
0 <sup>-</sup>	1 <sup>+</sup>	2995.8(8)	459.4(4)	2536.4(7)	
(1 <sup>+</sup> ,2 <sup>-</sup> ,3 <sup>+</sup> )	2 <sup>+</sup>	3317.9(7)	2403.7(6)	914.2(3)	
6 <sup>-</sup> ,(4 <sup>-</sup> )	4 <sup>-</sup> ,(2 <sup>-</sup> )	3423.7(6)	2649.6(4)	774.1(4)	
(1 to 5) <sup>-</sup>	4 <sup>-</sup> ,(2 <sup>-</sup> )	3619.0(6)	2649.6(4)	969.4(4)	
3 <sup>+</sup>	2 <sup>+</sup>	3670.7(7)	2403.7(6)	1267.0(8)	
(2,3,4)	4,(2 <sup>-</sup> )	3693.3(4)	2649.6(4)	1043.9(3)	100(20)
	3 <sup>-</sup>		2616.6(4)	1076.3(7)	46(15)
(0 to 4) <sup>+</sup>	2 <sup>+</sup>	3707.3(7)	2403.7(6)	1303.6(3)	
2 <sup>-</sup>	2 <sup>+</sup>	3816.8(9)	2403.7(6)	1413.1(7)	
2 <sup>-</sup>	3 <sup>-</sup>	3935.6(6)	2616.6(4)	1319.0(5)	
1 to 5 <sup>-</sup>	4706.3(9)	3619.0(6)	1087.3(7)		

TABLE I:  $\gamma$ -ray energies and intensities observed in the current experiment. The initial ( $J_i$ ) and final ( $J_f$ ) angular momenta and initial ( $E_i$ ) and final ( $E_f$ ) state energies are also listed [23].

TABLE II: The unshifted  $\gamma$ -ray energy, initial velocity  $v_0/c$ , average velocity  $\bar{v}/c$  and attenuation factor for excited states in  $^{38}\text{K}$ .

$E_x$ (keV)	$E_0$ (keV)	$v_0/c$	$\bar{v}/c$	$F(\tau)$	$\overline{F(\tau)}$
1698	1568.0(4)	0.0094	0.0081(4)	0.87(4)	0.87(4)
2404	1944.3(5)	0.0091	0.0079(3)	0.87(4)	0.89(3)
	2273.1(14)		0.0090(8)	0.95(6)	
2830	426.3(4)	0.0089	0.0050(7)	0.56(8)	0.55(4)
	2700.3(8)		0.0049(4)	0.55(4)	
2996	2536.4(7)	0.0088	0.0075(4)	0.85(5)	0.85(5)
3671	1267.0(4)	0.0085	0.0069(5)	0.81(5)	0.81(5)

$E_x$	Present work		Collins [7]		Hasper [8]		Engmann [9]		Weighted average
(keV)	$F(\tau)$	$\tau$ (fs)	$F(\tau)$	$\tau$ (fs)	$F(\tau)$	$\tau$ (fs)	$F(\tau)$	$\tau$ (fs)	$\tau$ (fs)
1698	0.87(4)	109±29	0.85(5)	82±35	0.953(8)	65±15	54±25	71±11	
2404	0.89(3)	95±22	0.86(7)	76±50	0.933(6)	90±25	54±25	80±13	
2830	0.55(4)	457±63	0.66(7)	205 <sup>+65</sup> <sub>-55</sub>	0.76(4)	280±70			312±37
2996	0.85(5)	130±40			0.79(2)	220±50			165±31
3671	0.81(5)	160±50	0.83(8)	95±55	0.94(5)	<150			131±37

TABLE III: The attenuation factors  $F(\tau)$  and extracted lifetimes compared with previous work.